Pergamon

Geochimica et Cosmochimica Acta, Vol. 66, No. 18, pp. 3327–3337, 2002

0016-7037/02 $22.00 + .00

PII S0016-7037(02)00916-X

Post-shock annealing of Miller Range 99301 (LL6): Implications for impact heating of ordinary chondrites

ALAN E. RUBIN*

Institute of Geophysics and Planetary Physics, University of California, Los Angeles, CA 90095-1567, USA

(*Received February* 7, 2002; *accepted in revised form April* 22, 2002)

Abstract—MIL 99301 is an LL chondrite that has experienced successive episodes of thermal metamorphism, shock metamorphism and annealing. The first recognizable petrogenetic episode resulted in thermal metamorphism of the rock to petrologic type 6 (as indicated by homogeneous olivine compositions, significant textural recrystallization, and the presence of coarse grains of plagioclase, metallic Fe-Ni and troilite). The source of heat for this thermal episode is not identified. The rock also experienced shock metamorphism to shock stage ~S4 as indicated by extensive silicate darkening (caused by the dispersion within silicate grains of thin chromite melt veins and trails of metallic Fe-Ni and troilite blebs), polycrystalline troilite, myrmekitic plessite, a relatively high occurrence abundance (OA) of metallic Cu (3.6), the presence of numerous chromite-plagioclase assemblages, and coarse grains of low-Ca clinopyroxene with polysynthetic twinning. The shock event responsible for these effects must have occurred after the epoch of thermal metamorphism to type-6 levels; otherwise the polycrystallinity of the troilite would have disappeared and the low-Ca clinopyroxene would have transformed into orthopyroxene. Despite abundant evidence of strong shock, olivine and plagioclase in MIL 99301 exhibit sharp optical extinction, consistent with shock stage S1 and characteristic of an unshocked rock. This implies that an episode of post-shock annealing healed the damaged olivine and plagioclase crystal lattices and thereby changed undulose extinction into sharp extinction. The rock was probably annealed to metamorphic levels approximating petrologic type 4; more significant heating would have transformed the low-Ca clinopyroxene into orthopyroxene. It is not plausible that an episode of annealing occurring after the epoch of thermal metamorphism could have been caused by the decay of ^{26}Al because this isotope would have decayed away by that time. Impact heating is a more plausible source of post-metamorphic annealing of rocks in the vicinity of impact craters on low-density, high-porosity asteroids with rubble-pile structures.

1. INTRODUCTION

More than 99% of well-characterized ordinary chondrite (OC) falls are classified into petrologic types 3.6 to 6 or are type-3 breccias containing some type-4 to −6 material (Grady, 2000). All of these rocks have experienced significant degrees of thermal metamorphism. The identification of the mechanism(s) responsible for heating the OC parent asteroids is among the major unsolved problems of planetary science. Most researchers favor heating by the decay of the short-lived radionuclide ^{26}Al (e.g., Urey, 1955; Fish et al., 1960; Lee et al., 1976; Grimm and McSween, 1993) and have cast a critical eye on collisional heating models (Wood and Pellas, 1991; Keil et al., 1997; McSween et al., 2002).

However, Rubin (1995) suggested that impact-heating models are supported by the positive correlation between petrologic type and shock stage among OC (a fact also noted by Stöffler et al., 1991, on the basis of more limited data) and by the invariably high petrologic types of unmelted chondritic clasts within OC impact-melt breccias. The presence of metamorphosed impact-melt rock clasts in many OC fragmental breccias indicates that impact events occurred before or at the same time as thermal metamorphism (Rubin et al., 1983). Also consistent with impact-heating models is the observation that those chondrite groups with many metamorphosed members (H, L, LL, EH, EL, CK) also have at least a moderate number of shocked members (Stöffler et al., 1991; Rubin et al., 1997; Rubin, 1992), whereas groups with no metamorphosed members (CI, CO, CM, CR) have few or no shocked members (Scott et al., 1992). The main exception is the CV group, which contains no metamorphosed members but does include several members that are shock stage S3 (Scott et al., 1992).

Kring et al. (1999) and Rubin et al. (2001) modeled the Portales Valley H chondrite as a rock that experienced significant impact melting, loss of metal from silicate clasts, and pooling of metal in thick veins. Although the olivine grains must have been significantly shocked during this process, most of the olivine grains in Portales Valley exhibit sharp optical extinction characteristic of an unshocked rock (i.e., shock stage S1; Stöffler et al., 1991). This apparent discrepancy can be resolved if we assume that the olivine crystal lattices were healed by elemental diffusion during postshock annealing (i.e., by annealing due to shock residual heating or waste heat). Other OC that have been inferred to have undergone postshock annealing include the S1 meteorites H6 Kernouvé (which contains a series of elongated metal masses that appear to be parts of a partially obliterated shock vein; Hutson, 1989) and H5 Allegan (which exhibits major silicate darkening due to the dispersion of numerous curvilinear trails of small opaque blebs within silicate grains; Rubin, 1992).

Postshock annealing processes are not confined to asteroid-size bodies. Lunar poikilitic-granoblastic rocks appear to have been formed by shock processes followed by burial in close

* Author to whom correspondence should be addressed (aerubin@ucla.edu).

proximity to impact melts beneath the floor of an impact crater (Cushing et al., 1999). Shocked quartz grains with planar deformation features (PDF) from some terrestrial impact craters have undergone recrystallization during thermal metamorphism resulting in crystallization of small quartz grains along the PDF (Leroux et al., 1994).

I report here observations on the Miller Range 99301 ordinary chondrite (hereafter MIL 99301) that was collected as a single 4037.3-g stone in Antarctica. This rock provides unambiguous evidence of postshock annealing. It seems likely that the annealing experienced by this rock was caused by impact heating.

2. SAMPLES AND ANALYTICAL PROCEDURES

Five thin sections of MIL 99301 (sections 12, 22, 23, 24 and 25) from opposite ends of the whole rock were studied microscopically in transmitted and reflected light. Grain sizes were determined microscopically using a calibrated reticle. Mineral analyses were made with the Cameca "Camebax-microbeam" electron microprobe at UCLA on section 12 using natural and synthetic standards, 20-s counting times, and PAP corrections (the Cameca version of ZAF corrections). Modal analyses of section 12 were made in reflected light with a petrographic microscope using an automated point counter.

3. RESULTS

3.1. Weathering Grade

MIL 99301 is of weathering class B and fracturing class A (McBride et al., 2001), indicating that the rock exhibits moderate surface rustiness and minor fracturing. Thin section examination reveals that there is only minor brown staining of silicates; <1% of silicate grains have been affected. Although more than 95% of the metallic Fe-Ni grains are free of limonite, in some regions limonite rinds up to 35-μm thick coat the metal grains. In rare instances, metal grains have been largely to completely replaced by limonite. Also present in these weathered regions are a few thin limonite veins filling fractures in the mafic silicate grains. I classify the meteorite as weathering stage W1 (Wlotzka, 1993).

3.2. Chondrite Group

The mean compositions of randomly analyzed olivine (Fa28.1) and low-Ca pyroxene (Fs23.2Wo1.2) grains in MIL 99301 (Table 1) show it to be an LL chondrite. These values are within the established ranges of LL chondrites (Fa26.6– 32.4; Fs23.2– 25.7; Rubin, 1990; Gomes and Keil, 1980). Unmelted chromite grains (i.e., matrix grains that are not part of chromite-plagioclase assemblages) also have compositions (Table 2) within the LL-chondrite range (Fig. 191 of Brearley and Jones, 1998), although the mean FeO content (31.7 wt.%) of MIL 99301 chromite is somewhat below the LL4 to 6 range (~34 to 35 wt.%).

Other phases have compositions that are moderately different from those in equilibrated LL chondrites. The mean composition of plagioclase in MIL 99301 (Ab83.1Or5.8; Table 2) is less sodic and more potassic than the mean value for LL chondrites (Ab85.9Or3.6; Van Schmus and Ribbe, 1968). The mean kamacite Co content (12 mg/g; Table 3) is slightly below the compositional range of equilibrated LL chondrites (14.2 to 370 mg/g Co), but appreciably greater than that of L (7.0 to 9.5 mg/g Co) chondrites (Rubin, 1990). Although a few so-called L/LL chondrites (e.g., Bjurböle, Holbrook) also contain kamacite with 12 mg/g Co (Rubin, 1990), as I discuss below, the compositions of plagioclase and kamacite in MIL 99301 may have been modified by shock processes and, thus, may not be precise indicators of chondrite-group classification.

Table 1. Compositions (wt. %) of mafic silicates in MIL 99301.

no. of grains	olivine 12	low-Ca pyx 13	diopside 3
SiO_2	38.6 ± 0.2	56.2 ± 0.6	54.9 ± 0.4
TiO_2	<0.04	0.16 ± 0.05	0.36 ± 0.05
Al_2O_3	<0.04	0.15 ± 0.04	0.45 ± 0.05
Cr_2O_3	<0.04	0.13 ± 0.04	0.76 ± 0.08
FeO	25.4 ± 0.3	15.2 ± 0.7	5.2 ± 0.3
MnO	0.45 ± 0.04	0.47 ± 0.04	0.21 ± 0.02
MgO	36.4 ± 0.2	27.7 ± 0.03	16.2 ± 0.2
CaO	<0.04	0.64 ± 0.09	22.4 ± 0.2
Na_2O	<0.04	<0.04	0.43 ± 0.01
total	100.8	100.7	100.9
endmember	Fa28.1 ± 0.2	Fs23.2 ± 0.9	Fs8.3 ± 0.6
		Wo1.2 ± 0.2	Wo45.7 ± 0.4

Although mean chondrule sizes increase with increasing degree of whole-rock recrystallization (as small chondrules become integrated with matrix material), the mean chondrule size in MIL 99301 is 700±200 μm (n=31), close to the mean diameter of chondrules in LL3 chondrites (~600 μm; Rubin, 2000) and much greater than the mean chondrule diameters in L3 or H3 chondrites (~500 and ~300 μm, respectively; Rubin, 2000).

Metallic Fe-Ni occurs as individual grains of kamacite as well as intergrowths of kamacite-taenite, kamacite-troilite, kamacite-taenite-troilite and kamacite-taenite-chromite. The modal abundance of metallic Fe-Ni in MIL 99301 (4.2 wt.%; Table 4) is near the mean of LL chondrite falls (3.6 wt.%; Table 5 of Jarosewich, 1990) and lower than the range of L falls (5.3 - 10.4 wt.%; Jarosewich, 1990).

Table 2. Compositions (wt. %) of plagioclase and chromite in the matrix and inside chromite-plagioclase assemblages in MIL 99301.

	plagioclase		chromite	
	matrix	c-p asmblg	matrix	c-p asmblg
no. of grains	10	5	8	9
SiO_2	66.3 ± 0.4	65.1 ± 1.0	<0.04	0.14 ± 0.19
TiO_2	0.05 ± 0.05	0.07 ± 0.05	3.1 ± 0.5	1.9 ± 0.7
Al_2O_3	21.6 ± 0.2	21.8 ± 0.3	5.7 ± 0.4	11.6 ± 2.7
Cr_2O_3	<0.04	0.28 ± 0.27	55.4 ± 0.5	51.5 ± 2.4
FeO	0.49 ± 0.19	0.59 ± 0.24	31.7 ± 0.5	29.0 ± 0.7
MnO	<0.04	<0.04	0.54 ± 0.04	0.48 ± 0.09
MgO	<0.04	<0.04	1.7 ± 0.2	3.9 ± 0.4
CaO	2.2 ± 0.1	2.7 ± 0.4	<0.04	0.13 ± 0.05
Na_2O	8.8 ± 0.4	8.3 ± 0.5	<0.04	<0.04
K_2O	0.92 ± 0.42	0.87 ± 0.51	<0.04	<0.04
total	100.4	99.7	98.1	98.8
endmember	Ab83.1 ± 2.7	Ab80.3 ± 1.8		
	Or5.8 ± 2.5	Or5.5 ± 3.2		

c-p asmblg = chromite-plagioclase assemblages

Table 3. Compositions (wt. %) of opaque phases in MIL 99301.

mineral	kamacite			taenite		troilite	pent
description no. of grains	coarse kam 6	kam in plessite 3	coarse tn 5	rim of plessite 1	tn near small tr grains 1	coarse grains 7	patches in tr 1
Fe	93.7 ± 1.0	96.6 ± 1.5	64.2 ± 1.2	63.0	60.5	63.1 ± 0.38	46.6
Ni	5.6 ± 0.9	3.0 ± 0.6	36.3 ± 1.6	37.6	40.0	<0.04	19.5
Co	1.2 ± 0.4	1.2 ± 0.2	0.56 ± 0.37	0.11	0.06	<0.04	0.39
S	<0.04	<0.04	<0.04	<0.04	<0.04	36.8 ± 0.10	33.6
Cr	<0.04	<0.04	<0.04	<0.04	<0.04	<0.04	<0.04
total	100.5	100.8	101.1	100.7	100.6	99.9	100.1

kam = kamacite; tn = taenite; tr = troilite; pent = pentlandite

The preponderance of the mineralogical/petrological properties (olivine and low-Ca pyroxene compositions, chondrule size, metallic Fe-Ni abundance) indicates that MIL 99301 is an LL-group chondrite.

3.3. Texture and Petrologic Type

The homogeneity of the olivine (Fa28.1±0.2 mol.%; n=12) and low-Ca pyroxene (Fs23.2±0.9; n=13) compositions in MIL 99301 is consistent with that of an equilibrated (i.e., type-4 to −6) LL chondrite (e.g., Van Schmus and Wood, 1967; Rubin, 1990). This compositional equilibration is matched by textural recrystallization of the whole rock (Fig. 1). MIL 99301 contains recrystallized chondrules of all major textural types: barred olivine (BO), radial pyroxene (RP), granular olivine-pyroxene (GOP), cryptocrystalline (C), type-I and -II porphyritic olivine (PO), porphyritic pyroxene (PP) and porphyritic olivine-pyroxene (POP). Chondrules are generally well integrated with the matrix (Fig. 1). Also present are a few clear interstitial 100-μm-size grains of polysynthetically twinned plagioclase and smaller (20 to 50-μm-size) plagioclase grains that lack twinning; plagioclase grains ≥50 μm in size are characteristic of type-6 chondrites (Van Schmus and Wood, 1967). Grains of metallic Fe-Ni (140±150 μm, n=50) and sulfide (90±100 μm, n=130) in MIL 99301 are similar in mean size to those in type-5 and −6 OC (120 μm and 75 to 80 μm, respectively) (Table 2 of Rubin et al., 2001). These features, particularly the coarse plagioclase grains, indicate that MIL 99301 is a type-6 LL chondrite (as originally classified by McBride et al., 2001).

Although MIL 99301 contains coarse grains of orthopyroxene, consistent with its type-6 classification (Van Schmus and Wood, 1967), also present are several coarse (100 × 100 μm to 130 × 400 μm) grains of low-Ca clinopyroxene exhibiting polysynthetic twinning and inclined extinction (Fig. 2a,b). The mean composition of the low-Ca clinopyroxene grains (Fs23.7Wo1.4) is not appreciably different from the mean low-Ca pyroxene composition of the rock (Fs23.2Wo1.2). The occurrence of low-Ca clinopyroxene grains in MIL 99301 is inconsistent with the mineral assemblage expected in a normally metamorphosed, unbrecciated type-6 chondrite. The implications of these grains for the petrogenetic history of the rock are discussed below.

Table 4. Modal abundances of major phases in MIL 99301.

	vol. %	wt. %	mean LL (wt. %)*
silicate	92.5	88.2	88.4
troilite	5.2	7.1	5.8
metallic Fe-Ni	1.8	4.2	3.6
chromite	0.40	0.6	0.8
limonite	0.02	0.03	0.0
metallic Cu	1.8×10^{-4}	4.7×10^{-4}	4×10^{-4}
total	99.9	100.1	99.9
no. of points	4158	4158	
area (mm^2)	130	130	

Weight percent was converted into vol. % using the following specific gravities: silicate, 3.3; troilite, 4.67; metallic Fe-Ni, 7.95; chromite, 4.7; limonite, 4.28; metallic Cu, 8.95. The modal abundance of metallic Cu was estimated by direct measurement of the sizes of the four occurrences in thin section MIL 99301,12.

* Mean LL chondrite data based on CIPW norm of the oxide components of the mean composition of LL falls (Jarosewich, 1990) added to the abundances of metallic Fe-Ni and troilite determined by Jarosewich (1990). Total includes (in wt. %): 0.2% ilmenite (from CIPW norm) and 0.2% C, 0.2% P_2O_5 and 0.7% H_2O (Jarosewich, 1990). The abundance of metallic Cu was estimated from Rubin (1994).

3.4. Metallography

Some metal-troilite assemblages in MIL 99301 consist of adjacent 100 to 300-μm-size patches of kamacite (12 mg/g Co,

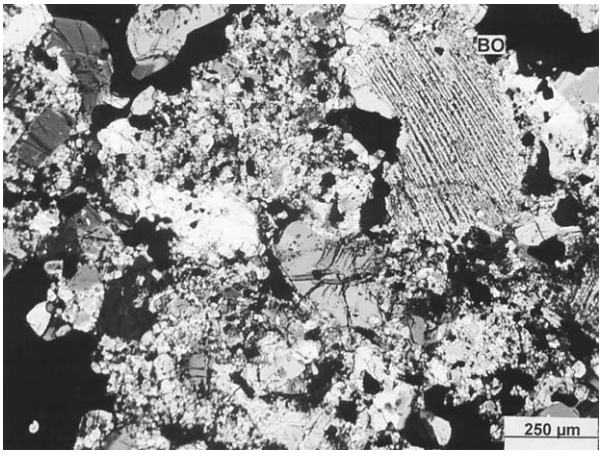

Fig. 1. Recrystallized texture of MIL 99301 showing a barred olivine (BO) chondrule fragment (upper right) and a few coarse grains of mafic silicates (center and left center) integrated with recrystallized matrix. Crossed-nicols.

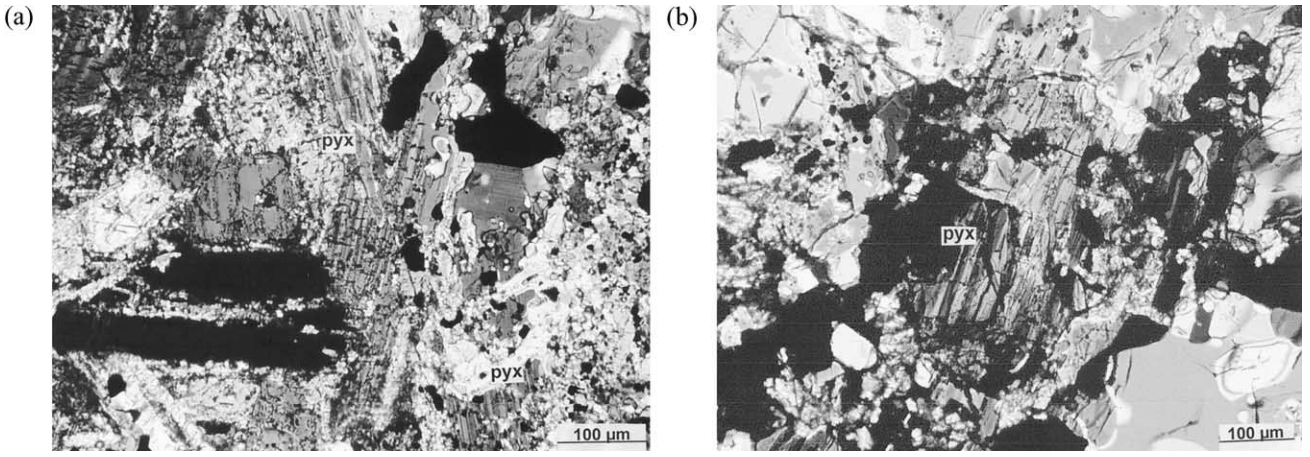

Fig. 2. Polysynthetically twinned low-Ca clinopyroxene grains. (a) A cluster of elongated low-Ca clinopyroxene (pyx) grains (center) surrounded mainly by mafic silicate grains. (b) Coarse low-Ca clinopyroxene (pyx) grain (center) flanked by mafic silicate and opaque grains (black). Both images are in crossed-nicols.

56 mg/g Ni), Ni-free troilite, and plessite (Fig. 3a,b); in some cases, similarly sized patches of taenite (0.6 mg/g Co, 400 mg/g Ni) containing small (5 to 30 μm) irregular grains of troilite (with 0.25 wt.% Ni) are also present (Fig. 3b).

The plessitic regions consist of a myrmekitic intergrowth of small (1 to 20-μm) irregular, wormy or finger-like kamacite grains (in some cases resembling cuneiform or runic letters) surrounded by taenite (Fig. 3c,d); the small kamacite grains contain 12 mg/g Co and 30 mg/g Ni. The plessitic regions themselves have 5 to 100-μm-thick (typically 25 μm) taenite rims containing 1.1 mg/g Co and 376 mg/g Ni (Table 3).

3.5. Shock Features

MIL 99301 exhibits extensive silicate darkening caused by numerous 100 to 200-μm-long curvilinear trails of 1 to 3-μm-size blebs of metallic Fe-Ni and troilite within silicate grains (Fig. 4a,b). These trails are inferred to have formed during shock events when localized temperatures exceeded that of the Fe-FeS eutectic (988°C) and Fe-FeS melt was injected into fractures in the mafic silicate grains (Rubin, 1992). Subsequent annealing healed the fractures and sealed the curvilinear trails of opaque blebs inside the silicate grains.

Several grains of coarsely polycrystalline troilite occur (Fig. 5). The troilite grains range from 200 to 600 μm in size and typically consist of two large adjacent patches of troilite with different crystal orientations. Some of the polycrystalline troilite grains contain 10 $\times$ 30- to 20 $\times$ 50-μm-size patches of pentlandite (Fig. 5). Bennett and McSween (1996a) pointed out that polycrystalline troilite can be used as an indicator of shock pressure. Shock-recovery experiments show that troilite becomes polycrystalline at shock pressures of 35 to 60 GPa (Schmitt et al., 1993); the lower limit corresponds to shock stage S4-S5 (Stöffler et al., 1991).

Rubin (1994) defined a petrographic property called occurrence abundance (OA) equal to 100 $\times$ [(number of occurrences)/mm^2]. He found that ordinary chondrites with metallic Cu OA values $\geq$2.5 tended to be more shocked (i.e., have a higher mean shock stage) than those with metallic Cu OA values $<$2.5. Sixteen occurrences of metallic Cu (2 to 20 μm in size) were identified in the five thin sections of MIL 99301 (total surface area, 440 mm^2). The metallic Cu grains occur within metallic Fe-Ni and adjacent to 3 to 20-μm-size irregularly shaped troilite grains. The metallic Cu OA value of 3.6 is consistent (although not exclusively so) with the meteorite being appreciably shocked (Rubin, 1994).

Most grains of chromite in unshocked equilibrated OC are irregular, rounded or blocky grains surrounded by mafic silicates (with or without adjacent minor plagioclase) or coarse grains adjacent to (or, in some cases, enclosed within) metallic Fe-Ni or troilite. There are many examples of chromite grains that are incompletely surrounded by mafic silicates and adjacent to small grains of metallic Fe-Ni and/or troilite. MIL 99301 contains such chromite assemblages (Fig. 6a), but in addition, there are numerous 25 to 300-μm-size patches of 0.2 to 10-μm-size euhedral, subhedral, anhedral and rounded chromite grains surrounded by plagioclase (Fig. 6b-d). Similar chromite-plagioclase assemblages have been reported in the Ramsdorf, Portales Valley and Smyer OC impact-melt breccias (Begemann and Wlotzka, 1969; Rubin et al., 2001; Rubin, 2002) and in the shock-stage S5 chondrite Kyushu, L6 (Ashworth, 1985). Keil et al. (1977) reported chromite droplets dispersed within maskelynite in the shock-stage S6 chondrite Paranaiba L6. Other shocked chondrites that contain chromite-plagioclase assemblages include L6 Jartai (S4), L6 La Criolla (S4), L6 NWA 108 (S4) and the Rose City H5 impact-melt breccia (S6) (A.E. Rubin, unpublished observations, 2001).

Present within some silicate grains are 5 to 300-μm-long veins composed of chromite blebs (equant 1-μm-size grains) and/or 0.5-μm-thick chromite needles (e.g., Fig. 6d). Some chromite veins cut across each other at angles of 30 to 90°.

The compositions of the phases in the chromite-plagioclase assemblages tend to differ from those of unmelted grains elsewhere in MIL 99301 (e.g., Fig. 6a). Assemblage chromite grains that are completely surrounded by plagioclase contain significantly more Al_2O_3 (11.6$\pm$2.7 vs. 5.7$\pm$0.4 wt.%), more

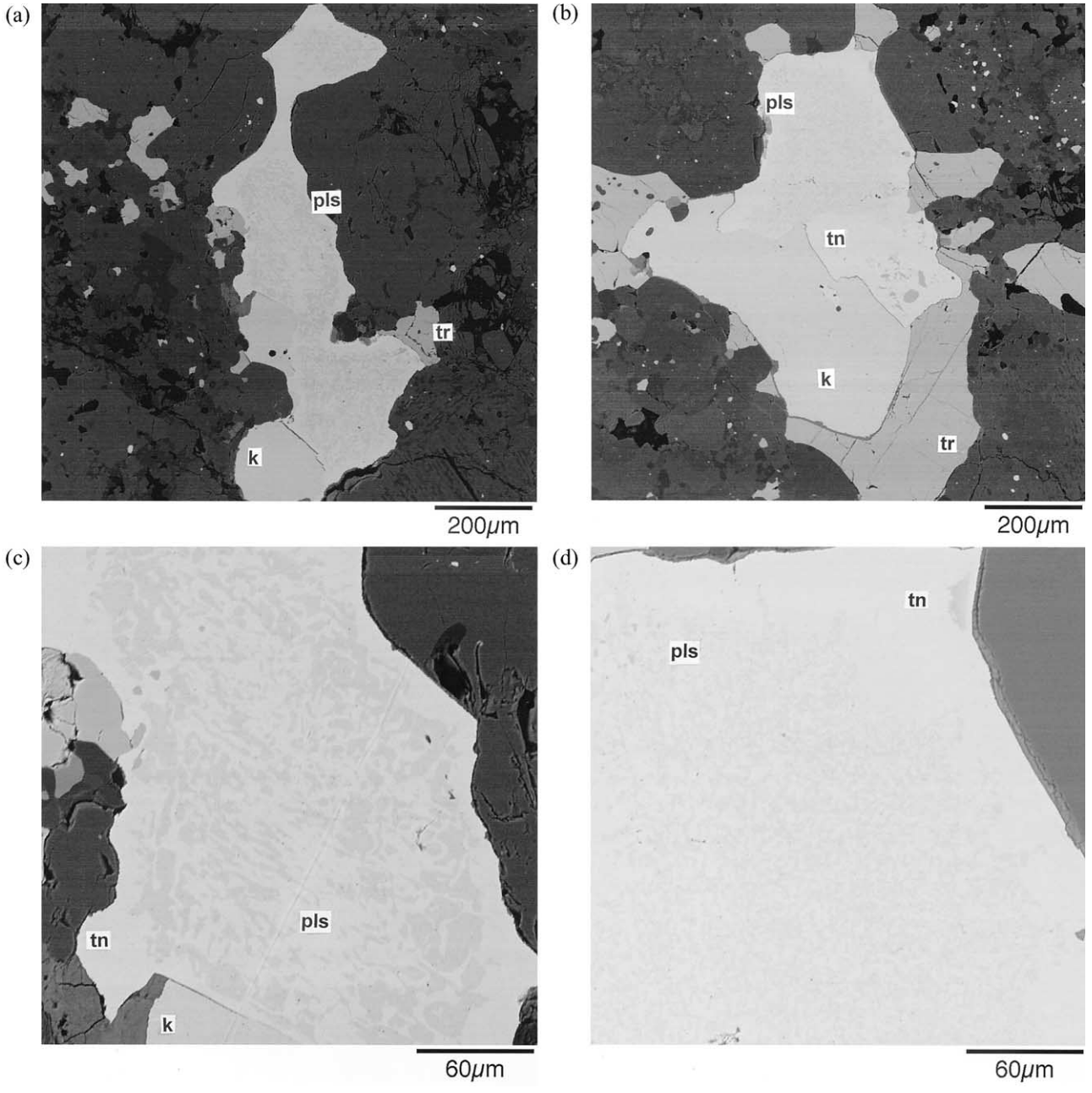

Fig. 3. Back-scattered electron images of opaque assemblages. (a) Assemblage consisting of troilite (tr, medium gray), kamacite (k, light gray), and plessite (pls) (that contains taenite (white) surrounding irregular, wormy kamacite grains). Dark gray areas around the assemblage consist mainly of mafic silicate grains. (b) Assemblage consisting of troilite (tr, medium gray), kamacite (k, light gray), taenite (tn; white, containing small troilite grains), and plessite (pls) (that contains taenite (white) surrounding irregular kamacite grains). (c) Higher-magnification image of the plessite (pls) portion of the assemblage in (a) showing taenite (tn; white) surrounding irregular kamacite grains (light gray). A large patch of kamacite (k) occurs at bottom of image. (d) Higher-magnification image of the plessite (pls) portion of the assemblage in (b) showing taenite (tn; white) surrounding irregular kamacite grains (light gray).

MgO (3.9±0.4 vs. 1.7±0.2 wt.%) and less TiO_2 (1.9±0.7 vs. 3.1±0.5 wt.%) than unmelted matrix chromite grains (Table 2). The chromite grain with the highest Al_2O_3 content (17.4 wt.%) is the largest chromite grain in the assemblage in Fig. 6c. Other chromite grains in this assemblage contain 9 to 13 wt.% Al_2O_3. Chromite grains at the edge of the assemblages that are only partly surrounded by plagioclase (e.g., the small chromite grains at the right edge of the assemblage in Fig. 6d) tend to have the same compositions as the unmelted chromite grains outside the assemblages.

Plagioclase in these assemblages contains marginally more CaO (2.4 to 3.3 wt.%, mean 2.7±0.4 wt.%) and Cr_2O_3

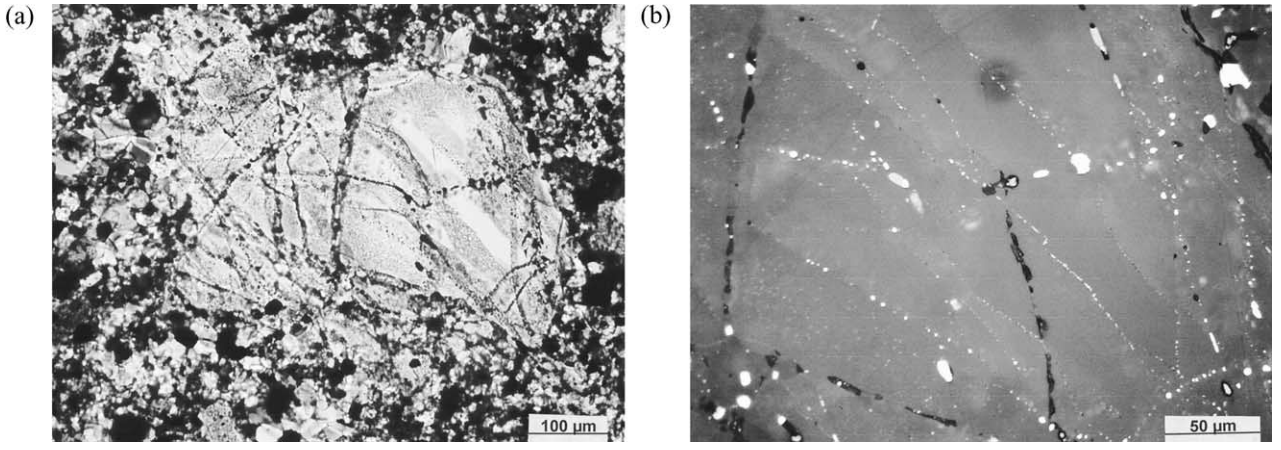

Fig. 4. Olivine grain exhibiting extensive darkening due to the dispersion of intersecting curvilinear trails of tiny blebs of metallic Fe-Ni and sulfide through the grain interior. (a) Opaque trails (black) at the surface of the olivine grain are parts of opaque veins that cut obliquely through the olivine grain. Such veins are characteristic of heavily shocked chondrites. Transmitted light. (b) Higher-magnification image of the olivine grain in (a) showing that the curvilinear trails within the olivine consist of small blebs of metal and sulfide. Reflected light.

(0.28±0.27 wt.%) than coarse crystalline plagioclase grains in the same rock (2.1 to 2.3 wt.%, mean 2.2±0.1 wt.% CaO; <0.04 wt.% Cr_2O_3) (Table 2).

4. DISCUSSION

4.1. Thermal and Shock History

4.1.1. Formation of opaque assemblages

I examined some weakly shocked (shock-stage S3) LL6 falls to determine the petrographic characteristics of their opaque assemblages to use as a comparison to those in MIL 99301. Dongtai and Min-Fan-Zhun (Rugao) contain opaque assemblages consisting of 100 to 250-μm-sized patches of kamacite, taenite and troilite; no plessite is present. These assemblages are of similar size and mineralogy to those in MIL 99301. It therefore seems likely that kamacite-troilite-plessite assemblages in MIL 99301 resembled the assemblages in Dongtai and Min-Fan-Zhun before shock metamorphism. Successive hypervelocity shock waves (including shock waves reflecting off grain boundaries) can lead to appreciable heating resulting from highly localized stress concentrations (Rinehart, 1968). Thus, the plessitic regions in the MIL 99301 assemblages may have formed by the localized shock melting of abutting (possibly intergrown) kamacite and taenite grains during an impact event that left other kamacite and troilite grains in the assemblage unmelted.

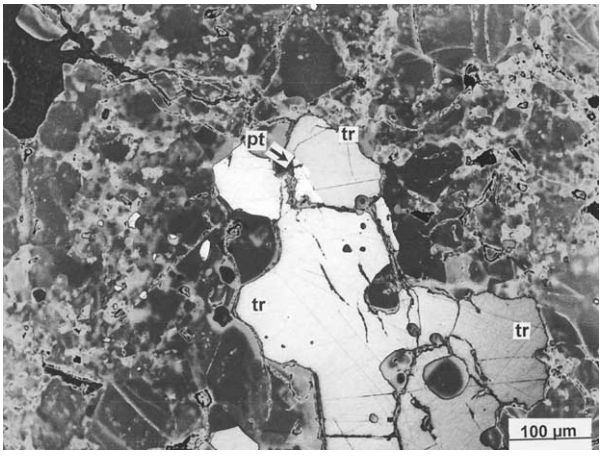

Fig. 5. Polycrystalline troilite grain with included pentlandite. The bulk of the troilite (tr) is a single crystal (light gray), a second crystal of troilite forms a darker-shaded patch at the center of the image (medium gray). Pentlandite (pt, white) occurs immediately to the left of the second troilite crystal. Mafic silicate grains (medium to dark gray) surround the sulfide assemblage. Reflected light.

The mean Co content of coarse kamacite grains in MIL 99301 (12 mg/g) is slightly below the kamacite range in LL4 to 6 chondrites (14.2 to 370 mg/g Co; Table 3 of Rubin, 1990). The mean Ni content of coarse kamacite grains in MIL 99301 (56 mg/g) is nearly identical to that in LL6 chondrite kamacite (54.9 mg/g Ni; Table 5 of Rubin, 1990). Kamacite within the MIL 99301 plessite regions has appreciably lower Ni (30 mg/g) and higher Fe (966 mg/g) than coarse kamacite grains (56 mg/g Ni and 937 mg/g Fe) (Table 3) suggesting that kamacite within the plessite regions has been affected by reduction of FeO from adjacent silicate grains and concomitant acquisition of additional Fe. If this is correct, then the Co concentration in the kamacite within the plessite regions must have been initially higher than 12 mg/g. It is possible that reduction of FeO has affected all of the kamacite in MIL 99301, lowering the Co concentrations from some value ≥14 mg/g and the Ni concentrations from some value >56 mg/g.

4.1.2. Plagioclase

The coarse crystalline plagioclase grains have a mean composition (Ab83.1Or5.8) different (more calcic, more potassic, and less sodic) from the LL chondrite mean (Ab85.9Or3.6) and slightly outside the LL chondrite range (Ab83.3–88.5 Or0.9–5.1; Van Schmus and Ribbe, 1968). It is possible that this difference is an artifact; Na mobilization under the electron beam is a particular problem in analyses of shocked plagioclase (Jeanloz and Ahrens, 1976).

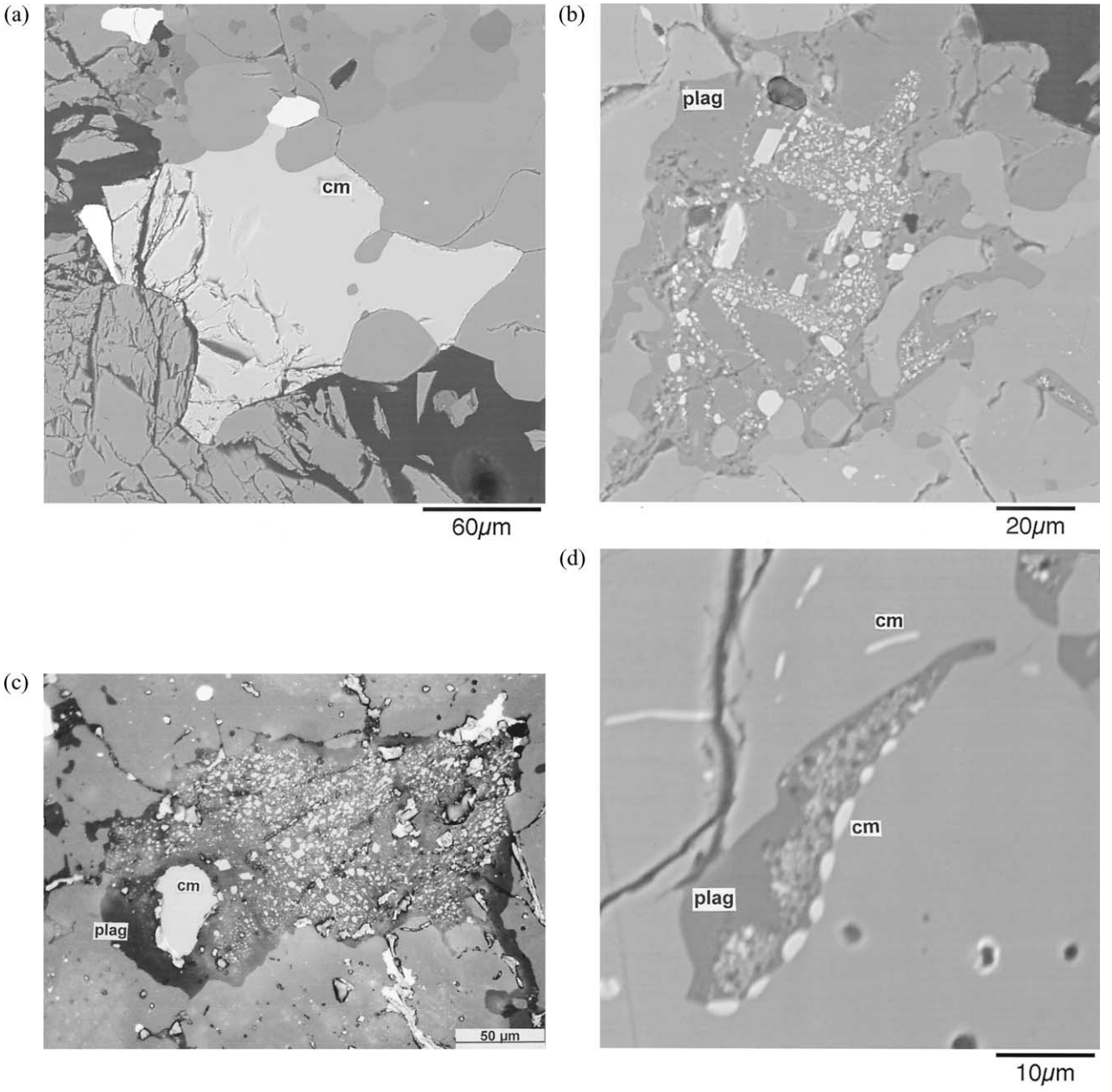

Fig. 6. Chromite and chromite-plagioclase assemblages. (a) Irregular chromite (cm) grain (light gray) surrounded by mafic silicate grains (medium gray) and adjacent to small grains of metallic Fe-Ni (white). BSE image. (b) Chromite-plagioclase assemblage consisting of a few moderate-size chromite grains (light gray) and discrete patches of numerous small chromite grains, all embedded in plagioclase (plag; dark gray). Mafic silicates surround the assemblage. BSE image. (c) Chromite-plagioclase assemblage consisting of one relatively coarse chromite (cm) grain (light gray, left) and numerous small rounded to partly faceted chromite grains surrounded by an irregular patch of plagioclase (plag; dark gray). Mafic silicates (medium gray) surround the assemblage. Reflected light. (d) Small chromite-plagioclase assemblage containing chromite (cm) blebs (light gray) at the right margin of the assemblage, inclusion-free plagioclase (plag) (dark gray) at the left margin, and a fine-grained mixture of chromite and plagioclase in the center and center-right of the assemblage. Also present are small thin plagioclase-free chromite veinlets that are near (but not connected to) the assemblage. BSE image.

On the other hand, Rubin (1992) found that stoichiometric plagioclase in shocked OC tends to be more calcic than plagioclase in unshocked OC. This is consistent with the results of Schaal and Hörz (1977) who found that experimentally shocked plagioclase and experimentally produced maskelynite are, on average, more calcic and less sodic than unshocked plagioclase. These differences probably result from the low impedance of plagioclase to shock compression (Schaal et al., 1979); during shock events, plagioclase can be melted preferentially, an event plausibly followed by fractionation (involving evaporative loss of Na_2O) and recrystallization (Rubin, 1992).

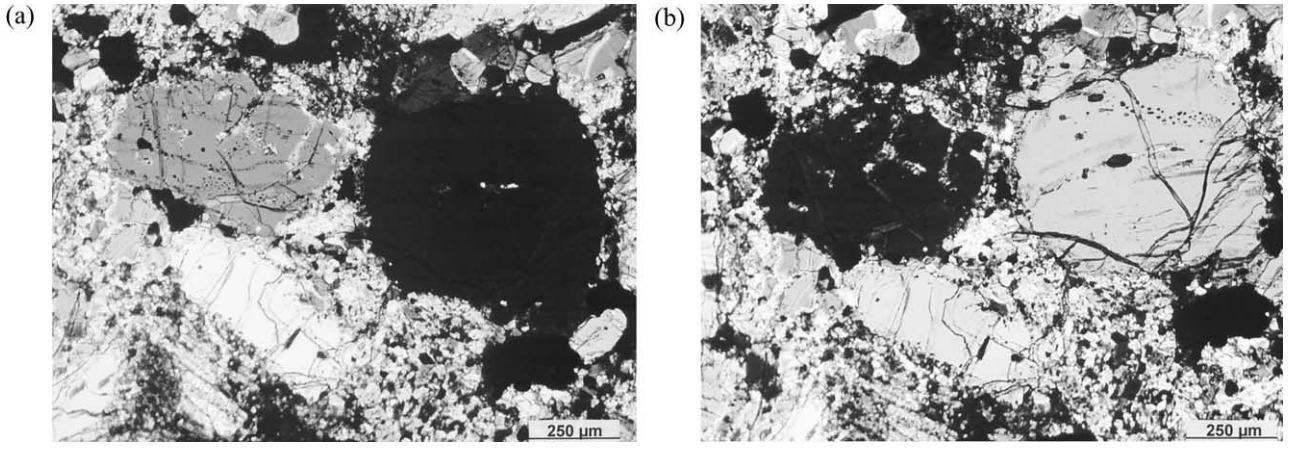

Fig. 7. Three adjacent coarse olivine grains exhibiting sharp optical extinction characteristic of shock stage S1. (a) The grain at right is extinct at one position of the rotating stage. The remaining two olivine grains do not exhibit undulose extinction. (b) At a different position of the rotating stage, the olivine grain at left is extinct and the grains at right and bottom are not. Both images in crossed nicols.

4.1.3. Formation of low-Ca clinopyroxene

The coarse grains of low-Ca clinopyroxene in MIL 99301 (Fig. 2) resemble the low-Ca clinopyroxene phenocrysts of pyroxene chondrules in type-3 and −4 OC (e.g., Fig. 4.5 of Dodd, 1981). However, low-Ca clinopyroxene could not have survived metamorphism to type-6 (or even type-5) levels without transforming into orthopyroxene; the clinoenstatite-orthoenstatite transition occurs at ≤630°C (Boyd and England, 1965; Grover, 1972), significantly lower than the equilibration temperatures of type-5 or type-6 chondrites (700 to 750°C and 820 to 930°C, respectively; Dodd, 1981; Olsen and Bunch, 1984). Therefore, the grains in MIL 99301 probably formed by shock heating and quenching. Hornemann and Müller (1971) and Stöffler et al. (1991) found that clinopyroxene lamellae parallel to (100) form within orthopyroxene grains at shock pressures of ~5 GPa. Rubin et al. (1997) examined equilibrated OC and found that such grains are common among shock-stage S3 chondrites and rare or absent in shock-stage S1 and S2 chondrites.

Because MIL 99301 is unbrecciated, it is unlikely that the low-Ca clinopyroxene grains were incorporated into the rock during an impact event as a component of type-3 material (which would have included well-defined chondrules, some containing glassy mesostases). Clasts of such type-3 material have not been observed in MIL 99301.

4.1.4. Ambiguities of shock stage assignment

The shock features of MIL 99301 yield inconsistent shock stage assignments. High shock stages are indicated by several parameters. These include (1) extensive silicate darkening, characteristic of S3-S6 chondrites (Rubin, 1992), (2) polycrystalline troilite, characteristic of S4-S5 (Bennett and McSween, 1996a; Schmitt et al., 1993), (3) a high metallic Cu occurrence abundance (OA), consistent with S3-S6 (Rubin, 1994), (4) chromite-plagioclase assemblages and thin chromite veins, characteristic of S4-S6 (this study), and (5) low-Ca clinopyroxene grains, characteristic of S3-S6 (Rubin et al., 1997). These parameters indicate that MIL 99301 was shocked to S4-S6 levels. However, if the rock had been shocked to S5 or S6 levels, plagioclase would have transformed into maskelynite (Stöffler et al., 1991). Recrystallization of maskelynite during annealing would not have produced coarse homogeneous single crystals of plagioclase as occurs in MIL 99301, but rather aggregates of fine-grained crystals with numerous vesicles (Ostertag and Stöffler, 1982). Thus, it appears that MIL 99301 was shocked to ~S4 levels.

According to Stöffler et al. (1991), olivine grains in an S3 chondrite should exhibit planar fractures and undulatory extinction; at S4, mosaicism begins to develop. Plagioclase develops undulatory extinction at S3 and becomes partially isotropic at S4 (Stöffler et al., 1991).

However, plagioclase and olivine in MIL 99301 have properties indicating a whole-rock apparent shock stage of S1. Plagioclase grains in MIL 99301 are crystalline, not glassy, and exhibit sharp optical extinction. Nearly every olivine grain in MIL 99301 exhibits sharp optical extinction (Fig. 7a,b); the olivine grains also lack planar fractures and planar deformation features. The rock thus appears to be unshocked according to the criteria of Stöffler et al. (1991). As described in the following section, these inconsistent shock indicators can be explained if the MIL 99301 whole rock experienced shock followed by annealing.

4.1.5. Petrogenesis

Here I interpret MIL 99301 as a rock that has experienced a complex history involving successive identifiable episodes of thermal metamorphism, shock metamorphism and postshock annealing.

MIL 99301 underwent thermal metamorphism to type-6 levels (820 to 930°C; Olsen and Bunch, 1984) as indicated by the rock's recrystallized texture (Fig. 1), coarse plagioclase grains, large grains of metallic Fe-Ni and troilite (Figs. 3 , 5), and uniform olivine and low-Ca pyroxene compositional distributions (Table 1). The heat source responsible for this episode of thermal metamorphism has not been identified.

Metallic Fe-Ni and troilite grains increase in size during thermal metamorphism (e.g., Wood, 1967). If the troilite had been polycrystalline before metamorphism, extensive recrystallization and growth of troilite during metamorphism to type-6 levels would have obliterated the polycrystallinity. Hence, the occurrence of polycrystalline troilite in MIL 99301 (Fig. 5) indicates that the rock was shocked after it was metamorphosed.

The absence of low-Ca clinopyroxene in unshocked, unbrecciated type-5 and −6 chondrites (Van Schmus and Wood, 1967) indicates that this phase could not have survived thermal metamorphism to type-5 or −6 levels. Thus, the low-Ca clinopyroxene grains in MIL 99301 (Fig. 2) must have formed after the rock was metamorphosed. The shock pressures must have been commensurate with at least shock-stage S3 (Rubin et al., 1997).

The principle of postshock annealing was recognized by Buchwald (1975) who pointed out that repeated impacts on a parent body could cause heating that would slowly dissipate through large volumes of buried material. The occurrence of olivine with sharp optical extinction (Fig. 7) (instead of undulatory extinction or mosaicism) and the occurrence of crystalline plagioclase with sharp optical extinction (instead of undulatory extinction or partial maskelynitization) indicate that MIL 99301 experienced postshock annealing. During the course of such annealing, the shock-induced damage of the olivine crystal lattice must have healed (Bauer, 1979). Experimental annealing of the shock-stage S5 Kyushu L6 chondrite for 90 h at 900°C and 1000°C caused fractures in the olivine grains to heal (Ashworth and Mallinson, 1985). Because elemental diffusion in olivine is faster than in low-Ca pyroxene (Freer, 1981), olivine grains can be healed at lower temperatures and/or shorter heating durations than those required to transform low-Ca clinopyroxene into orthopyroxene.

Several residual shock features in MIL 99301 are likely to have survived annealing. One such feature is silicate darkening (e.g., Fig. 4). Trails of small opaque blebs within olivine grains that were injected during shock events can become trapped within the olivine crystals when diffusion causes olivine recrystallization and healing of internal fractures. Thus, OC that exhibit major silicate darkening but also contain olivine grains with sharp optical extinction are likely to have experienced postshock annealing. One such rock is H5 Allegan, S1 (Table 2 of Rubin, 1992); another is Portales Valley, S1 (Kring et al., 1999; Rubin et al., 2001).

The solid/liquid distribution coefficient (K_d) of Cu is appreciably less than 1 in FeS-rich metallic Fe-Ni melts. During localized shock-melting of metal-troilite assemblages, taenite crystallizes first and Cu becomes supersaturated in the residual sulfide-rich liquid. Eventually, metallic Cu nucleates at high-surface-energy sites such as metal-troilite grain boundaries (Rubin, 1994). Once metallic Cu has nucleated it is very stable and should survive metamorphism even to type-6 levels. Thus, its occurrence in MIL 99301 is consistent with the rock having experienced postshock annealing.

Because chromite-plagioclase associations (e.g., Fig. 6) occur in many shocked chondrites, it seems likely that the impedance mismatch between chromite and plagioclase is sufficiently large to cause substantial shock reverberations at the grain boundaries between these phases. This would result in the localized melting of relatively large fractions of chromite. During annealing, the chromite and plagioclase might coarsen and recrystallize, but the assemblage should remain intact.

Although chromite needles and veinlets are plagioclase-free, most are located near chromite-plagioclase assemblages. It is possible that they formed from a melt that contained plagioclase that subsequently disappeared (either by evaporation or melt withdrawal into the chromite-bearing assemblages). In any case, the chromite needles and veinlets would remain after annealing.

Troilite grains coarsen during metamorphism, reaching their maximum size by type-5 levels (Table 2 of Rubin et al., 2001). I suggest that if polycrystalline troilite is reheated only to type-4 levels, there will be only moderate recrystallization. Annealing to this level may be sufficient to create single crystals from very fine adjacent troilite grains, but insufficient to affect coarsely polycrystalline textures. The occurrence of coarse polycrystalline troilite in MIL 99301 (Fig. 5) seems consistent with postshock annealing to type-4 metamorphic levels.

Low-Ca clinopyroxene is abundant in type-3 OC. During thermal metamorphism to type-4 levels, low-Ca clinopyroxene remains common because diffusion is still relatively sluggish at these only moderately elevated temperatures (~600 to 700°C; Dodd, 1981). However, by the time petrologic type-5 levels are reached (at temperatures of ~700 to 750°C; Dodd, 1981), monoclinic pyroxene has been transformed into orthopyroxene. The degree of completeness of the transformation depends on the amount of orthopyroxene intergrown with the low-Ca clinopyroxene initially (Brearley and Jones, 1993). [Experiments at higher temperatures (1100°C) show some reversion of clinoenstatite to orthoenstatite in as little as 5 h (Coe and Kirby, 1975). At temperatures of 700 to 750°C, reversion must take appreciably longer.] The presence of low-Ca clinopyroxene in MIL 99301 (Fig. 2) indicates that the postshock annealing episode was more akin to metamorphism to type-4 levels than to type-5 levels (consistent with the preservation of polycrystalline troilite).

Because of rapid elemental diffusion in olivine, even type-4-level metamorphism is sufficient to equilibrate olivine compositions (e.g., Keil and Fredriksson, 1964; Rubin, 1990). It is probably also sufficient to heal damaged olivine crystal lattices and transform crystals with undulose or mosaic extinction into grains with sharp extinction (e.g., Fig. 7).

4.2. Implications for the Mechanism Responsible for Metamorphosing Ordinary Chondrites

Live ^{26}Al was present in the early solar system; the signature of its decay product (excess ^{26}Mg) has been identified in refractory inclusions and chondrules (e.g., Lee et al., 1976; Russell et al., 1996; Kita et al., 1998; Mostefaoui et al., 1999). Recent thermal models of OC parent bodies (e.g., Bennett and McSween, 1996b) assume that metamorphic cooling to Pb blocking temperatures required ~60 Ma for type-6 chondrites (Göpel et al., 1994). These models predict parent bodies with very large proportions of approximately uniformly heated type-6 material with thin veneers of less-metamorphosed type-3 to 5 material.

Such models cannot account for the heterogeneous heating

of the Portales Valley meteorite breccia (Rubin et al., 2001). This rock contains extensively melted material within a few centimeters of essentially unmelted material. Rubin et al. (2001) concluded that Portales Valley was not heated by the decay of ^{26}Al but was instead heated by a mechanism capable of causing non-uniform heating, i.e., by an impact event (e.g., French, 1998).

In addition to being incompatible with extremely heterogeneous heating, ^{26}Al cannot be responsible for heating bodies after the 60-Ma-long epoch of thermal metamorphism (even if ^{26}Al decay had been responsible for "normal" metamorphic heating). After 60 Ma, the amount of ^{26}Al ($t_{½}$ = 0.72 Ma) remaining would be $\sim 2 \times 10^{-25}$ of the initial amount. The only viable heat source capable of causing postmetamorphic annealing is an impact. [Electromagnetic induction in the protosolar wind (e.g., Sonett et al., 1970; Herbert and Sonett, 1979) is ruled out because T Tauri stars blow off much of their mass at their poles, away from any planetesimals in the accretion disk (Wood and Pellas, 1991). Furthermore, Herbert (1989) estimated that the induction heating epoch lasted only $\sim 10^5$ a; thus, induction is not likely to have been an effective heat source at this late postmetamorphic stage in the history of MIL 99301.]

It is plausible that the same impact event that shocked MIL 99301 also buried the rock beneath the crater floor in the vicinity of impact melts or deposited the rock within a hot, thick ejecta blanket where annealing occurred. This process has happened in terrestrial impact craters. A residual component of the kinetic energy of the projectile is converted into thermal energy after the shock wave dissipates. The thermal energy is released from nonadiabatic decay of the shock wave (Raikes and Ahrens, 1979) and can induce static metamorphism in rocks beneath the crater floor. For example, maximum impact-induced temperatures within local regions within a few kilometers of the center of the Vredefort Dome in South Africa exceeded 1350°C (Gibson, 2002).

If chondritic rocks on asteroids could be emplaced near impact melts or buried in hot ejecta blankets without being significantly shocked, then the extrapolation could be made that impact heating is generally responsible for the thermal metamorphism of ordinary chondrites. This would not be a global heating process. Rocks could be significantly heated only in the vicinity of large impact craters. Many asteroids appear to be low-density, high-porosity bodies akin to rubble piles with densities as low as 1.2 g cm^{-3} (Veverka et al., 1999; Cheng and Barnouin-Jha, 1999; Bottke et al., 1999). In such bodies, kinetic energy is attenuated through relatively small volumes of material and efficiently converted into heat in the crater vicinity (e.g., Melosh, 1989; Housen and Holsapple, 1999). Impacts into asteroidal rubble piles might deposit thick insulating layers of finely crushed debris above strongly heated target rocks, allowing deeply buried rocks to cool slowly and anneal (Rubin, 1995). Because such impacts occur stochastically, materials on these asteroids could have been shocked and annealed several times.

Acknowledgments—I am grateful to the Antarctic Meteorite Working Group for providing the thin sections of MIL 99301. I also thank J.T. Wasson for useful comments and D.A. Kring, P.C. Buchanan and an anonymous referee for their helpful reviews. This work was supported in part by NASA Grant No. NAG5-4766 (A. E. Rubin).

Associate editor: W. U. Reimold

REFERENCES

Ashworth J. R. (1985) Transmission electron microscopy of L-group chondrites, 1: Natural shock effects. *Earth Planet. Sci. Lett.* **73,** 17–32.

Ashworth J. R. and Mallinson L. G. (1985) Transmission electron microscopy of L-group chondrites, 2: Experimentally annealed Kyushu. *Earth Planet. Sci. Lett.* **73,** 33–40.

Bauer J. F. (1979) Experimental shock metamorphism of mono- and polycrystalline olivine: A comparative study. *Proc. Lunar Planet. Sci. Conf.* **10,** 2573–2596.

Begemann F. and Wlotzka F. (1969) Shock induced thermal metamorphism and mechanical deformations in Ramsdorf chondrite. *Geochim. Cosmochim. Acta.* **33,** 1351–1370.

Bennett M. E. and McSween H. Y. (1996a) Shock features in iron-nickel metal and troilite of L-group ordinary chondrites. *Meteorit. Planet. Sci.* **31,** 255–264.

Bennett M. E. and McSween H. Y. (1996b) Revised model calculations for the thermal histories of ordinary chondrite parent bodies. *Meteorit. Planet. Sci.* **31,** 783–792.

Bottke W. F., Richardson D. C., Michel P., and Love S. G. (1999) 1620 Geographos and 433 Eros: Shaped by planetary tides. *Astron. J.* **117,** 1921–1928.

Boyd F. R. and England J. L. (1965) The rhombic enstatite-clinoenstatite inversion. In Carnegie Inst. Washington, Ann. Rpt. Dir. Geophys. Lab. **1964–65,** 117–120.

Brearley A. J. and Jones R. H. (1993) Chondrite thermal histories from low-Ca pyroxene microstructures: Autometamorphism vs. prograde metamorphism revisited. *Lunar Planet. Sci.* **24,** 185–186 (abstract).

Brearley A. J. and Jones R. H. (1998) Chondritic meteorites. In *Planetary Materials* (ed. J. J. Papike) Vol. 36, pp. 3–1–3–398. Mineralogical Society of America.

Buchwald V. F. (1975) *Handbook of Iron Meteorites*. Univ. Calif. Press, Berkeley, California 1418 pp.

Cheng A. F. and Barnouin-Jha O. S. (1999) Giant craters on Mathilde. *Icarus* **140,** 34–48.

Coe R. S. and Kirby S. H. (1975) The orthoenstatite to clinoenstatite transformation by shearing and reversion by annealing: Mechanism and potential applications. *Contrib. Mineral. Petrol.* **52,** 29–55.

Cushing J. A., Taylor G. J., Norman M. D., and Keil K. (1999) The granulitic impactite suite: Impact melts and metamorphic breccias of the early lunar crust. *Meteorit. Planet. Sci.* **34,** 185–195.

Dodd R. T. (1981) Meteorites—A Petrologic-Chemical Synthesis. Cambridge. 368, pp.

Fish R. A., Goles G. G., and Anders E. (1960) The record in the meteorites. III: On the development of meteorites in asteroidal bodies. *Astrophys. J.* **132,** 243–258.

Freer R. (1981) Diffusion in silicate minerals and glasses: A data digest and guide to the literature. *Contrib. Mineral. Petrol.* **76,** 440–454.

French B. M. (1998) *Traces of Catastrophe: A Handbook of Shock-metamorphic Effects in Terrestrial Meteorite Impact Structures*. LPI Contribution No. 954Lunar and Planetary Institute, Houston.

Gibson R. L. (2002) Impact-induced melting of Archean granulites in the Vredefort Dome, South Africa. I: Anatexis of metapelitic granulites. *J. Metamorphic Geol.* **20,** 57–70.

Gomes C. B. and Keil K. (1980) *Brazilian Stone Meteorites*. Univ, New Mexico 161pp.

Göpel C., Manhes G., and Allègre C. J. (1994) U-Pb systematics of phosphates from equilibrated ordinary chondrites. *Earth Planet. Sci. Lett.* **121,** 153–171.

Grady M. M. (2000) Catalogue of Meteorites. Fifth edition. Cambridge Univ. Press, 689 pp.

Grimm R. E. and McSween H. (1993) Heliocentric zoning of the asteroid belt by 26-Al heating. *Science* **259,** 653–655.

Grover J. E. (1972) The stability of low-clinoenstatite in the system $Mg_2Si_2O_6$-$CaMgSi_2O_6$. *EOS—Trans. Am., Geophys. Union.* **53,** 539 (abstract).

Herbert F. (1989) Primordial electrical induction heating of asteroids. *Icarus* **78,** 402–410.

Herbert F. and Sonett C. P. (1979) Electromagnetic heating of minor planets in the early solar system. *Icarus* **40,** 484–496.

Hornemann U. and Müller W. F. (1971) Shock-induced deformation twins in clinopyroxene. *Neues Jahrb. Mineral.* **6,** 247–256.
Housen K. R. and Holsapple K. A. (1999) Impact cratering on porous low-density bodies. *Lunar Planet. Sci.* **30,** abstract # 1228. Lunar and Planetary Institute.
Hutson M. (1989) Shock effects in H-group chondrites. *Lunar Planet. Sci.* **20,** 436–437 (abstract).
Jarosewich E. (1990) Chemical analyses of meteorites: A compilation of stony and iron meteorite analyses. *Meteoritics* **25,** 323–337.
Jeanloz R. and Ahrens T. J. (1976) Alkali mobility in shocked basalt. *Proc. Lunar Sci. Conf.* **7th,** 1623–1632.
Keil K. and Fredriksson K. (1964) The iron, magnesium, and calcium distribution in coexisting olivines and rhombic pyroxenes of chondrites. *J. Geophys. Res.* **69,** 3487–3515.
Keil K., Kirchner E., Gomes C. B., and Nelen J. (1977) Studies of Brazilian meteorites V. Evidence for shock metamorphism in the Paranaiba, Mato Grosso, chondrite. *Rev. Brasil. Geo.* **7,** 256–268.
Keil K., Stöffler D., Love S. G., and Scott E. R. D. (1997) Constraints on the role of impact heating and melting in asteroids. *Met. Planet. Sci.* **32,** 349–363.
Kita N. T., Nagahara H., Togashi S., and Morishita Y. (1998) New evidence of aluminum-26 from a ferrous-oxide-rich chondrule in Semarkona (LL 3.0). *Meteorit. Planet. Sci.* **33,** A83–A84 (abstract).
Kring D. A., Hill D. H., Gleason J. D., Britt D. T., Consolmagno G. J., Farmer M., Wilson S., and Haag R. (1999) Portales Valley: A meteoritic sample of the brecciated and metal-veined floor of an impact crater on an H-chondrite asteroid. *Meteorit. Planet. Sci.* **34,** 663–669.
Lee T., Papanastassiou D. A., and Wasserburg G. J. (1976) Demonstration of ^{26}Mg excess in Allende and evidence for. 26Al. *Geophys. Res. Lett.* **3,** 109–112.
Leroux H., Reimold W. U., and Doukhan J. -C. (1994) A TEM investigation of shock metamorphism in quartz from the Vredefort dome, South Africa. *Tectonophysics* **230,** 223–239.
McBride K., Satterwhite C., McCoy T., and Welzenbach L. (2001) List of newly classified Antarctic meteorites. *Ant. Met. Newslett.* **24,** 3–9 no.1.
McSween H. Y., Ghosh A., Grimm R. E., Wilson L. and Young E. D. (2002). Thermal evolution models of asteroids. In *Asteroids III* (ed. by R. Binzel), Univ. of Arizona Press, in press.
Melosh H. J. (1989) Impact Cratering: A Geologic Process. Oxford University Press. 245, pp.
Mostefaoui S., Kita N. T., Nagahara H., Togashi S., and Morishita Y. (1999) Aluminum-26 in two ferromagnesian chondrules from a highly unequilibrated ordinary chondrite: evidence of a short period of chondrule formation. *Meteorit. Planet. Sci.* **34,** A84 (abstract).
Olsen E. J. and Bunch T. E. (1984) Equilibration temperatures of the ordinary chondrites: A new evaluation. *Geochim. Cosmochim. Acta* **48,** 1363–1365.
Ostertag R. and Stöffler D. (1982) Thermal annealing of experimentally shocked feldspar crystals. *Proc. Lunar Planet. Sci. Conf.* **13,** A457-A463.
Raikes S. A. and Ahrens T. S. (1979) Post-shock temperatures in minerals. *Geophys. J. Roy. Astron. Soc.* **58,** 717–747.
Rinehart J. S. (1968) Intense destructive stresses resulting from stress wave interactions. In *Shock Metamorphism of Natural Materials* (eds. B. M. French and N. M. Short). Mono Book Corp. pp. 31–42.
Rubin A. E. (1990) Kamacite and olivine in ordinary chondrites: Intergroup and intragroup relationships. *Geochim. Cosmochim. Acta* **54,** 1217–1232.
Rubin A. E. (1992) A shock-metamorphic model for silicate darkening and compositionally variable plagioclase in CK and ordinary chondrites. *Geochim. Cosmochim. Acta* **56,** 1705–1714.
Rubin A. E. (1994) Metallic copper in ordinary chondrites. *Meteoritics* **29,** 93–98.
Rubin A. E. (1995) Petrologic evidence for collisional heating of chondritic asteroids. *Icarus* **113,** 156–167.
Rubin A. E. (2000) Petrologic, geochemical and experimental constraints on models of chondrule formation. *Earth Sci. Rev.* **50,** 3–27.
Rubin A. E. (2002) Smyer H-chondrite impact-melt breccia and evidence for sulfur vaporization. *Geochim. Cosmochim. Acta* **66,** 699–711.
Rubin A. E., Rehfeldt A., Peterson E., Keil K., and Jarosewich E. (1983) Fragmental breccias and the collisional evolution of ordinary chondrite parent bodies. *Meteoritics* **18,** 179–196.
Rubin A. E., Scott E. R. D., and Keil K. (1997) Shock metamorphism of enstatite chondrites. *Geochim. Cosmochim. Acta* **61,** 847–858.
Rubin A. E., Ulff-Møller F., Wasson J. T., and Carlson W. D. (2001) The Portales. Valley meteorite breccia: Evidence for impact-induced melting and metamorphism of an ordinary chondrite. *Geochim. Cosmochim. Acta* **65,** 323–342.
Russell S. S., Srinivasan G., Huss G. R., Wasserburg G. J., and MacPherson G. J. (1996) Evidence for widespread ^{26}Al in the solar nebula and constraints for nebula time scales. *Science* **273,** 757–762.
Schaal R. B. and Hörz F. (1977) Shock metamorphism of lunar and terrestrial basalts. *Proc. 8th Lunar Sci. Conf.*, 1697–1729.
Schaal R. B., Hörz F., Thompson T. D. and Bauer J. F. (1979) Shock metamorphism of granulated lunar basalt. *Proc. 10th Lunar Planet. Sci. Conf.*, 2547–2571.
Schmitt R. T., Deutsch A., and Stöffler D. (1993) Shock effects in experimentally shocked samples of the H6 chondrite Kernouvé. *Meteoritics* **28,** 431–432 (abstract).
Scott E. R. D., Keil K., and Stöffler D. (1992) Shock metamorphism of carbonaceous chondrites. *Geochim. Cosmochim. Acta* **56,** 4281–4293.
Sonett C. P., Colburn D. S., Schwartz K., and Keil K. (1970) The melting of asteroidal-sized bodies by unipolar dynamo induction from a primordial T Tauri sun. *Astrophys. Space Phys.* **7,** 446–488.
Stöffler D., Keil K., and Scott E. R. D. (1991) Shock metamorphism of ordinary chondrites. *Geochim. Cosmochim. Acta* **55,** 3845–3867.
Urey H. C. (1955) The cosmic abundances of potassium, uranium, and thorium and the heat balances of the Earth, the Moon, and Mars. *Proc. Natl. Acad. Sci.* **41,** 127–144.
Van Schmus W. R. and Ribbe P. H. (1968) The composition and structural state of feldspar from chondritic meteorites. *Geochim. Cosmochim. Acta* **32,** 1327–1342.
Van Schmus W. R. and Wood J. A. (1967) A chemical-petrologic classification for the chondritic meteorites. *Geochim. Cosmochim. Acta* **31,** 747–765.
Veverka J., Thomas P., Harch A., Clark B., Bell III J. F., Carcich B., Joseph J., Murchie S., Izenberg N., Chapman C., Merline W., Malin M., McFadden L., and Robinson M. (1999) NEAR encounter with asteroid 253 Mathilde: Overview. *Icarus* **140,** 3–16.
Wlotzka F. (1993) A weathering scale for the ordinary chondrites. *Meteoritics* **28,** 460 (abstract).
Wood J. A. (1967) Chondrites: Their metallic minerals, thermal histories, and parent planets. *Icarus* **6,** 1–49.
Wood J. A. and Pellas P. (1991) What heated the meteorite planets? In *The Sun in Time* (ed. C. P. Sonett, M. S. Giampapa, and M. S. Matthews), pp. 740–760:University of Arizona Press.